metals

MDPI

Article

Microstructure and High-Temperature Mechanical Properties of Mg-1Al-12Y Alloy Containing LPSO Phase

Qianlong Ren, Shuai Yuan, Jinhui Wang *, Deqing Ma, Wei Li and Lei Wang

Qinghai Provincial Key Laboratory of New Light Alloys, Qinghai Provincial Engineering Research Center of High Performance Light Metal Alloys and Forming, Qinghai University, Xining 810016, China
* Correspondence: ahui1004@163.com

Abstract: This paper describes our study on the effect of the long-period stacking order (LPSO) phase on the comprehensive mechanical properties of the as-cast Mg-1Al-12Y (wt. %) alloy. The microstructure and tensile mechanical properties of as-cast alloy and solution treatment alloy were evaluated. The results showed that α-Mg matrix, Al_2Y phase and β-$Mg_{24}Y_5$ phase were present in the as-cast alloy. After solution treatment, the β-$Mg_{24}Y_5$ phase in the alloy was dissolved and the LPSO phase was precipitated. The solution treatment did not cause grain growth or Al_2Y phase change, but the comprehensive mechanical properties of the alloy were significantly improved. This was mainly due to the precipitation of the LPSO phase in the solid solution alloy. In addition, the dissolution of the β-$Mg_{24}Y_5$ phase after solution treatment could also improve the mechanical properties. The improvement of the comprehensive mechanical properties of solution treatment alloys at room temperature was due to the dispersion strengthening caused by the intragranular LPSO phase dispersed within the alloy, which had a good blocking effect on the movement of dislocations. The ductility of the solid-solution alloy was greatly improved at a high temperature while maintaining high strength because the LPSO phase is kinked, the dislocation density was reduced, and more non-basal slip was activated during the high-temperature tension.

Keywords: RE magnesium alloy; LPSO phase; microstructure; mechanical properties

check for updates

Citation: Ren, Q.; Yuan, S.; Wang, J.; Ma, D.; Li, W.; Wang, L. Microstructure and High-Temperature Mechanical Properties of Mg-1Al-12Y Alloy Containing LPSO Phase. *Metals* **2023**, *13*, 158. https://doi.org/10.3390/met13010158

Academic Editor: Alberto Moreira Jorge Junior

Received: 7 November 2022
Revised: 8 December 2022
Accepted: 19 December 2022
Published: 12 January 2023

Copyright: © 2023 by the authors. Licensee MDPI, Basel, Switzerland. This article is an open access article distributed under the terms and conditions of the Creative Commons Attribution (CC BY) license (https://creativecommons.org/licenses/by/4.0/).

1. Introduction

Magnesium (Mg) alloy, as the lightest metal structure material, has great application potential in an industry where lightweight structures are key to reducing energy consumption [1–5]. However, due to the low strength and poor plasticity of Mg and Mg alloys, especially the poor high-temperature mechanical properties of Mg alloys, their further applications are limited. One study found that the properties of Mg alloys can be effectively improved by adding alloying elements [6]. The method of adding rare earth elements to Mg alloys to obtain special microstructures and excellent comprehensive mechanical properties at room temperature and high temperature has attracted a great deal of attention. In particular, the presence of the LPSO phase precipitated in rare earth Mg alloy can effectively improve the mechanical properties of the alloy at room temperature and high temperature, so ternary-element alloys such as Mg-Zn-Y [7,8] and Mg-Al-Gd [9,10] as well as multi-element alloys (e.g., Mg-Zn-Gd-Y-Zr [11,12]) of the LPSO phase can be precipitated and have been widely studied.

In addition, Mg-Al alloys have attracted the attention of many scholars due to their excellent mechanical properties, casting properties and low cost [13–15]. However, a large amount of β-$Mg_{17}Al_{12}$ phase is easily precipitated in the Mg-Al alloy system, and the elevated temperature stability is poor, which limits its application at high temperatures [16]. Since the solid solubility of Y element in Mg is high, and because the solid solubility decreases significantly with decreasing temperature, this can produce a strong aging strengthening effect. Adding the rare earth element Y [17] to Mg-Al alloy can form the Al_2Y

phase, and can also form LPSO phase after heat treatment; this can effectively improve the room-temperature and high-temperature mechanical properties of Mg-Al alloy. Wang prepared Mg-1Al-xY (x = 4, 6, 8) by a hot extrusion process. The results of this study showed that the addition of Y could significantly promote the precipitation of Al_2Y phase and effectively inhibit the precipitation of the β-$Mg_{17}Al_{12}$ phase [18]. At the same time, due to the dispersed distribution of the Al_2Y phase precipitated in the Mg alloy, not only were the grains of the alloy more refined, but the movement of dislocations were also hindered, effectively improving the mechanical properties of the alloy at room temperature. Through precise characterization by high-resolution transmission electron microscopy (HRTEM) [19–24], the types of LPSO phases have been found to mainly include 10H, 14H, 18R and 24R structures. The 18R and 14H LPSO phases are the most common of these structures. In addition, previous studies have shown [25–27] that the lamellar LPSO phase inside the grains in the Mg-Al-Y alloy is 18R-LPSO, which has a good coherent relationship with the Mg matrix, which is detrimental to the propagation of defects and is conducive to the plastic deformation of alloys. At the same time, the LPSO phase also has a higher elastic modulus than the Mg matrix, which can effectively play the role of second-phase strengthening. Su found that Mg-Gd-Al-Y alloy had good comprehensive mechanical properties, and had the best mechanical properties when the LPSO phase content was the largest. This was thought to be mainly due to the blocking effect of LPSO on dislocations in the matrix and its high Young's modulus [28].

The existence of the LPSO phase improves the mechanical properties of Mg-Al-Y alloy. However, the precipitation law and high-temperature strengthening mechanism of the LPSO phase in the Mg-Al-Y alloy are still unclear. In this work, the Mg-1Al-12Y alloy is melted by a traditional melting process, and the LPSO phase is obtained by solution treatment to study the microstructure and mechanical properties of Mg-1Al-12Y alloy as-cast and obtained by solution treatment to obtain the precipitation rule of LPSO phase and the high-temperature strengthening mechanism.

2. Experimental Produces

The raw materials of the Mg-1Al-12Y alloy (wt. %) were pure Mg (99.99%), pure aluminum (99.99%) and Mg-30 wt. % Y master alloy. Defect-free Mg-1Al-12Y (wt. %) alloy ingots were prepared by fusion casting. The alloy melt was held at 720 °C for 30 min, and then cast into a mold preheated at 100 °C with a mold size of φ500 mm × 1000 mm and cooled at room temperature. Subsequently, the samples required for the experiment were cut by the wire cutting method; the solution was treated at 450 °C for 1 h, 12 h and 24 h, separately, and then water quenched.

The microstructure, morphology and second-phase composition and distribution of alloys were characterized by optical microscopy (OM, Leica DMI3000I (Leica Microsystem, Wetzlar, Germany)), scanning electron microscopy (SEM, Merlin compact, (Carl Zeiss Microscopy Gmbh, Jena, Germany)), energy-dispersive spectroscopy (EDS, Merlin compact, (Lecia Microsystem, Welzlar, Germany)) and electron-backscattered diffraction (EBSD, Merlin compact, (Carl Zeiss Microscopy Gmbh, Jena, Germany)). As shown in Figure 1a, the observation surface of the OM and SEM samples of the alloys was perpendicular to the casting direction. The preparation process was as follows: First, the surface was sanded with sandpaper until there was no obvious scratch; then, 7% perchloric acid solution was used at −30 °C, polishing voltage 25 V, current 0.3 A; after electropolishing for 70 s, the surface was immediately washed with alcohol to clean the sample. After the perchloric acid alcohol solution was dropped on the surface for 5 s, the solution on the surface of the sample was rinsed with alcohol and dried. The phase compositions of the alloys were analyzed by X-ray diffraction analysis (XRD, Bruker D8-Advance A25, (Bruker, Billerica, MA, USA)). The scanning speed was 0.015°/s, the scanning angle was 20°~80°, the scanning voltage was 40 V and the current was 40 mA.

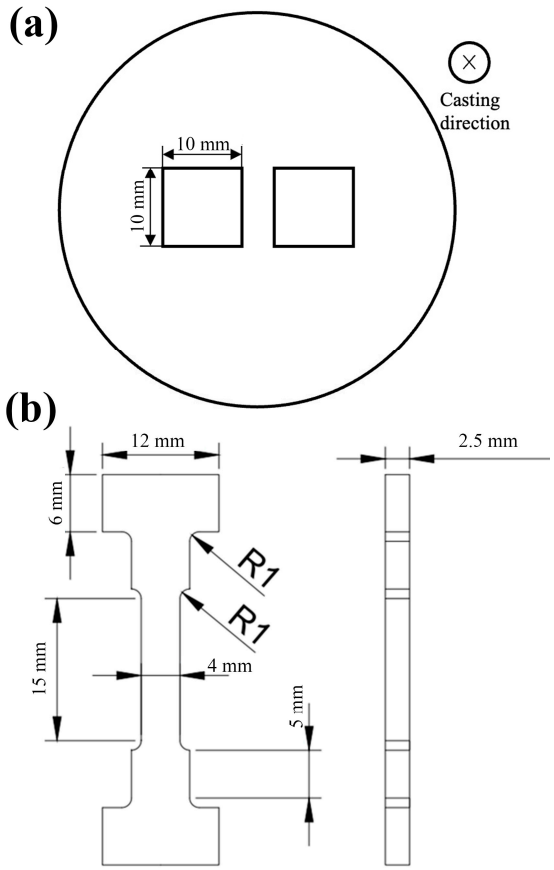


Figure 1. (**a**) Schematic diagram of sampling position and (**b**) dimension diagram of tensile specimen.

The mechanical properties of alloys were tested by a Vickers hardness tester (VH1102, BUEHLER, Chicago, IL, USA) and a universal testing machine (5982, Instron, (Norwood, MA, USA)). The hardness samples were 10 mm × 10 mm × 2 mm cuboids, and the preparation method of the test surface was the same as that of the SEM sample. The test load and dwell time were 100 g and 15 s, respectively, and 10 hardness values were measured for each sample and averaged. The size of the tensile specimen is shown in Figure 1b, and it is machined from the ingot by electric-discharge cutting method. The tensile rate of the sample is 0.2 mm/min. The high-temperature tensile temperature is 200 °C, and the heat preservation is 5 min.

3. Results

3.1. Microstructure of the As-Cast Alloy

The microstructure of the as-cast alloy is shown in Figure 2. The XRD pattern in Figure 2b shows that the as-cast alloy contains three phases, namely the α-Mg matrix, Al_2Y and β-$Mg_{24}Y_5$. After the EDS analysis of point A, as shown in Figure 2c, the ratio of the weight percentage of Al to Y was 1:2. Hence, the black massive phase in the OM image is the Al_2Y phase. It is observed that no LPSO phase is precipitated in the as-cast alloy, and the bulk Al_2Y phase is distributed in the grain boundaries and inside the grains (Figure 2a).

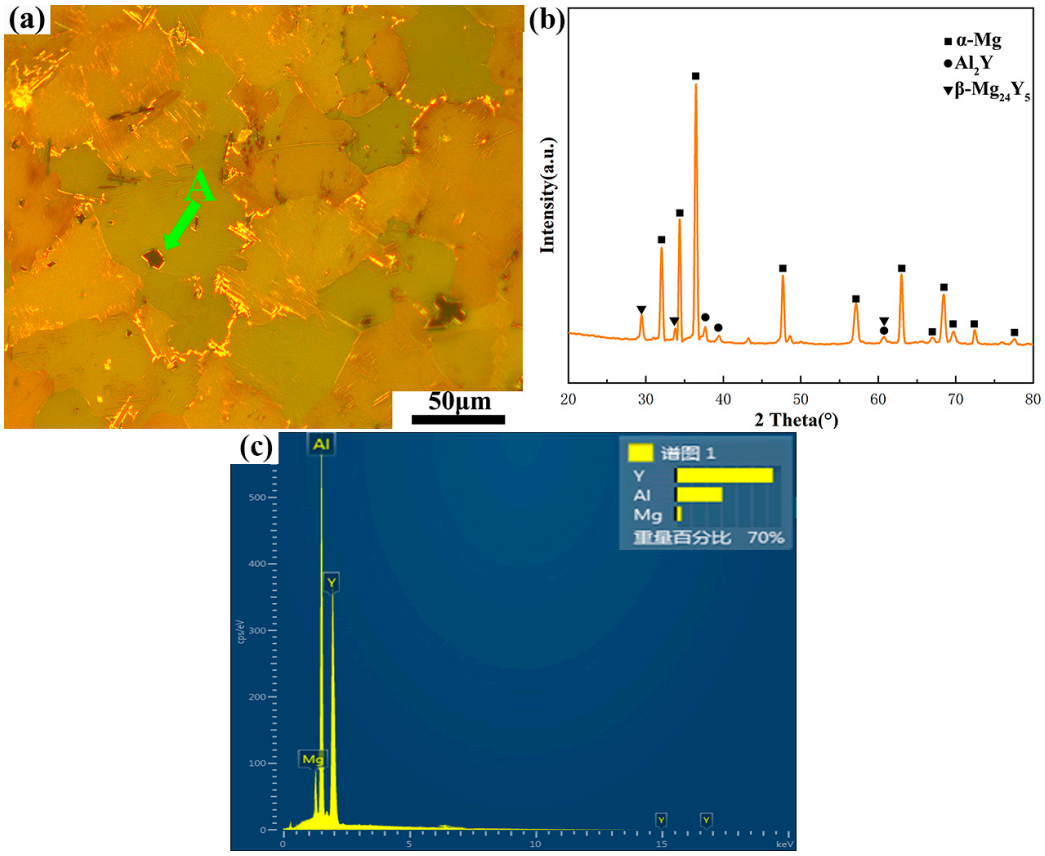


Figure 2. Microstructure of as-cast Mg-1Al-12Y alloy: (**a**) OM image, (**b**) XRD pattern and (**c**) EDS image of point A.

3.2. Microstructure of the Solution Treated Mg-1Al-12Y Alloy

Figure 3 shows the OM image and XRD patterns of Mg-1Al-12Y alloy after solution treatment at 450 °C at different times. From Figure 3d, it can be found that the diffraction peak of the LPSO phase appears in the spectrum of the solution-treated alloy, while the diffraction peak of the β-$Mg_{24}Y_5$ phase existing in the as-cast alloy disappears in the XRD pattern of the solution-treated alloy, which is due to the melting point of β-$Mg_{24}Y_5$ phase is lower, about 605 °C [12]. A blue rectangle marked the LPSO diffraction peak. It can be found from the local magnification that the diffraction peak width at half maximum of the LPSO phase of the alloy after 24 h solution treatment is 0.039° lower than that of the alloy after 12 h solution treatment. The relative intensity increases significantly, indicating that the content and size of the LPSO phase are increasing and growing. As shown in Figure 3a–c), under the polarizing mode of the optical microscope, it can be found that the alloy precipitates a large amount of gold intragranular layered LPSO phase and a small amount of interdendritic LPSO phase. The massive particles in the alloy are the Al_2Y phase, which is randomly distributed on the grain boundaries and within the grains of the alloy. It can be found that the number of grains with LPSO phase precipitation also increases with the prolongation of the solution time, and the size of the LPSO phase precipitated in the alloy also increases with the prolongation of the solution time. Figure 4 shows the line chart of grain size of as-cast alloy and solid solution alloys calculated by the software of Nano Measure. It was found that the grain size of the alloy did not change significantly after solution treatment.

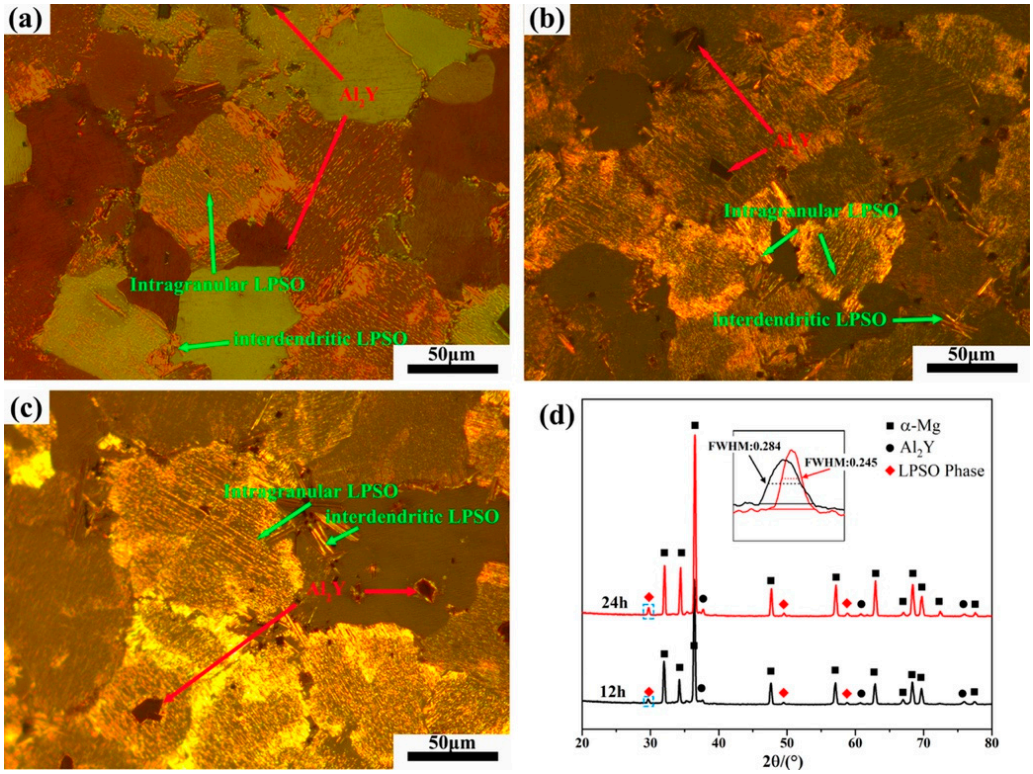


Figure 3. The OM images of solution-treated alloys. (**a**) 1 h, (**b**) 12 h, (**c**) 24 h and (**d**) XRD patterns.

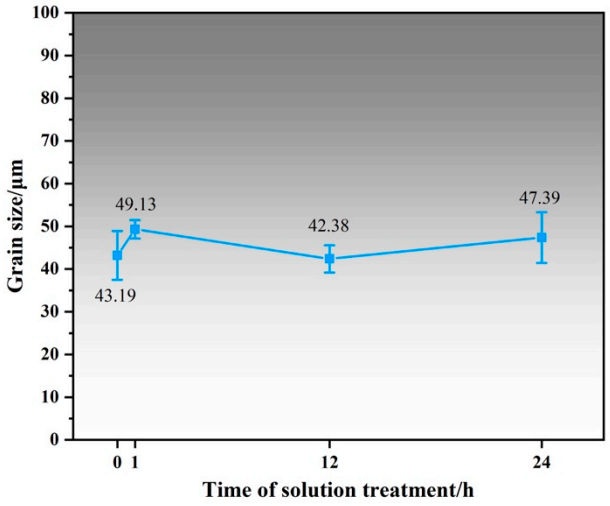


Figure 4. Grain size line chart of as-cast alloy and solid solution alloy.

The area fraction broken line diagram of the LPSO phase of the alloy after solution treatment at 450 °C for 1 h, 12 h and 24 h is shown in Figure 5 according to the statistics of Image Pro Plus software. It is found that with the prolongation of solution treatment time, the area fraction of the LPSO phase precipitated inside the alloy particles increased, which were 8.30%, 20.03% and 21.26%, respectively. This is the same conclusion drawn from the metallographic and XRD patterns shown in Figure 3.

Figure 6 shows the SEM images of the alloys solution-treated at 450 °C for 12 h and 24 h. It can be observed that the network β-$Mg_{24}Y_5$ phase at the grain boundary in the as-cast alloy is not found after the solution treatment, which further indicates that the β-$Mg_{24}Y_5$ phase in the alloy has been completely dissolved into the matrix. As shown in Figure 6a,b, the number, and size of the Al_2Y phase in the alloy did not change much, while the number of needle-like LPSO phases at the grain boundary decreased with the

solution time, and it is so small that it is difficult to observe the LPSO phase precipitated in the grains in the 200× SEM image. However, in the 600× SEM images, it can be observed that the fine LPSO phases are distributed parallel to each other inside the grains. Further amplification was carried out to observe better the distribution of the LPSO phase in the grains. The directions of the LPSO phases in different grains are marked with red lines parallel to the LPSO phases in Figure 6c,d. It is found that the layered LPSO phases within the same grain are parallel to each other, and the orientation of the LPSO phases between different grains is random.

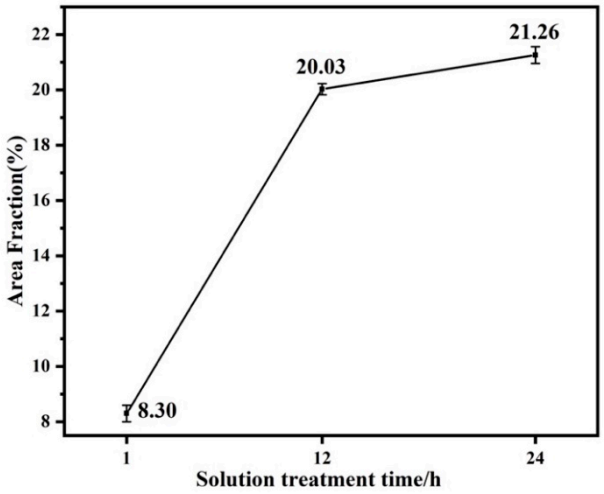


Figure 5. Area fraction line graph of LPSO Phase in Solid Solution Alloys.

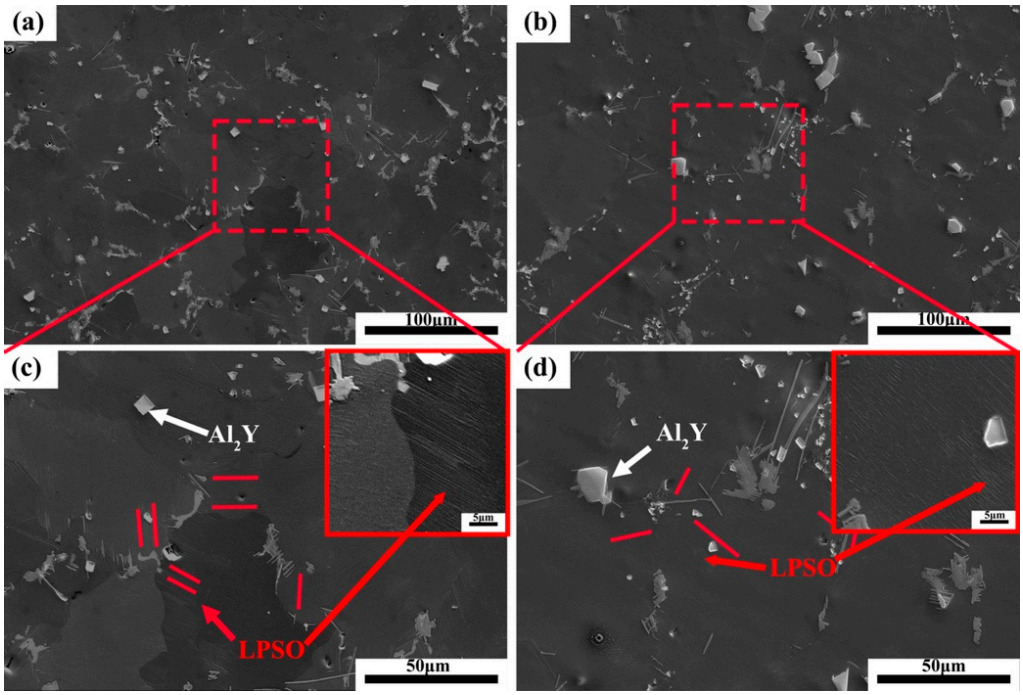


Figure 6. The SEM images of solution treatment alloys, (**a**,**c**) 12 h, (**b**,**d**) 24 h.

Figure 7 shows the IPF diagram, grain boundary diagram and pole diagram of the as-cast alloy and solution treatment for 12 h. From Figure 7a,d, it can be found that there is no grain preferred orientation in either as-cast alloy or solid solution alloy, and the white particles in Figure 7d are the LPSO phase. As shown in Figure 7b,e, the grain boundaries of the two alloys only have very few small angle grain boundaries. As shown in Figure 7c,f,

the alloys are all random textures. The texture strengths of as-cast alloy and solid solution alloy are 9.05 and 7.72, respectively. It is found that the texture strengths of the alloy decrease with the precipitation of the LPSO phase. As the grain size of the alloy after solution treatment for 12 h is the smallest difference from that of the as-cast alloy, the grains have no preferred orientation and the grain boundaries are basically the same. In addition, the area fraction of the LPSO phase precipitated after 24 h and 12 h solution treatment is basically the same, so the alloy with solution treatment after 12 h is selected for subsequent mechanical property testing.

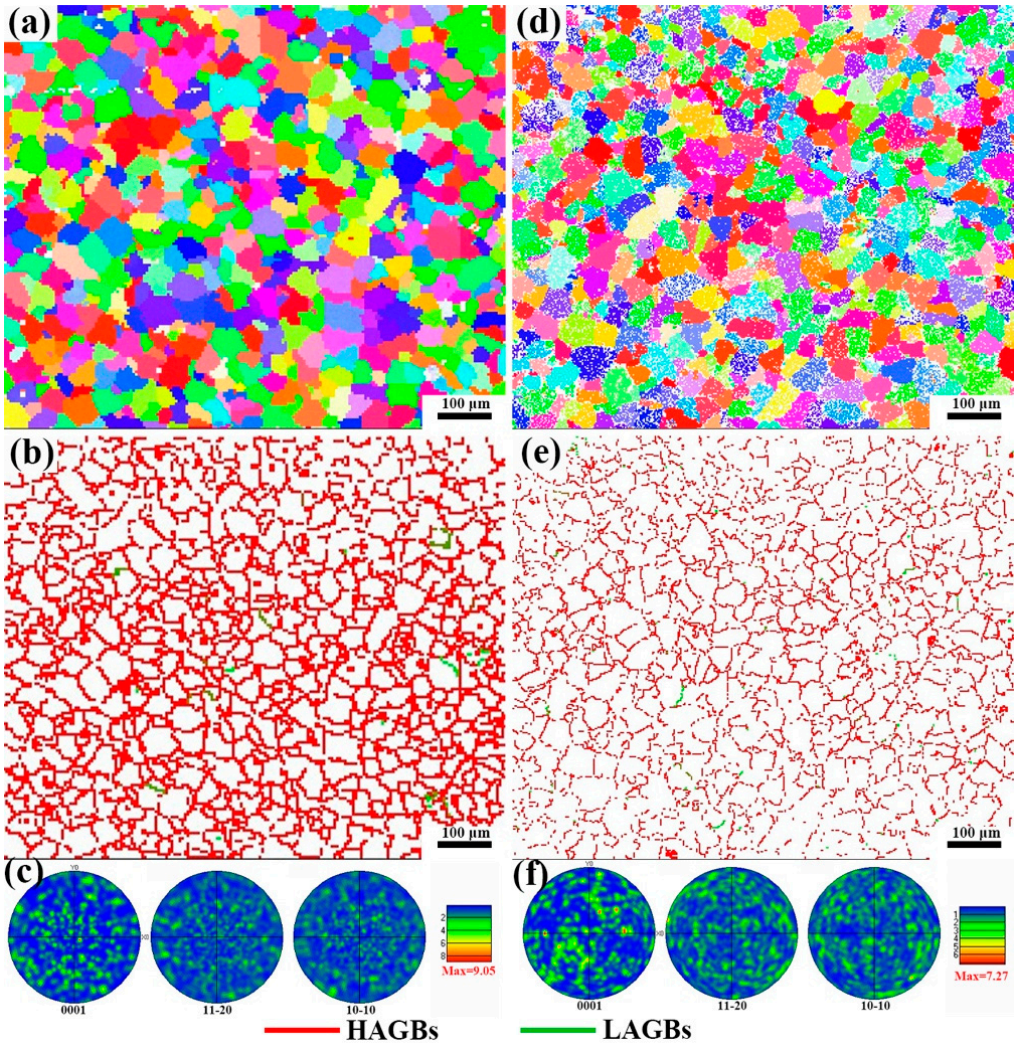


Figure 7. IPF image, grain boundary image and pole figure of as-cast alloy (**a**–**c**) and alloy after solution treatment for 12 h (**d**–**f**).

3.3. Mechanical Properties

After solution treatment at 450 °C, alloys with different LPSO contents were obtained, and then the hardness and tensile tests were carried out on the alloys with different LPSO contents. Figure 8 presents the Vickers hardness of the as-cast alloy and the solution-treated alloy. It can be found that the Vickers hardness decreases with the prolongation of solution treatment time. The reason why the Vickers hardness of the alloy after solution treatment is significantly lower than that of the as-cast alloy is that the network β-$Mg_{24}Y_5$ phase in the as-cast alloy disappears with the solution treatment. In addition, with the increase in the LPSO phase precipitated in the solid solution alloy, the hardness of the alloy also tends to decrease. It shows that the increase in the LPSO phase precipitation area fraction can effectively improve the mechanical properties of the alloy [29].

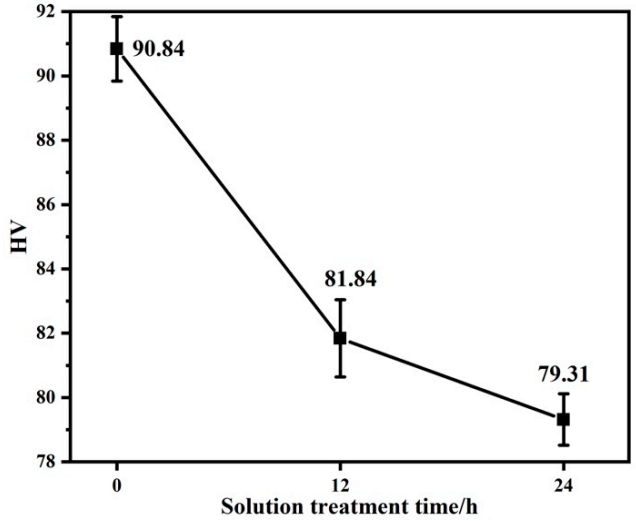


Figure 8. Hardness curves of alloys with different solution treatment times.

Figure 9 indicates the engineering stress–strain curve of the as-cast alloy stretched at room temperature (Alloy A), the alloy stretched at room temperature after solution treatment at 450 °C for 12 h (Alloy B) and the alloy stretched at 200 °C after solution treatment at 450 °C for 12 h (Alloy C). The corresponding mechanical properties are summarized in Table 1. It can be found that the UTS, TYS and EL of the as-cast alloy at room temperature are 156.99 MPa, 133.45 MPa and 4.2%, respectively. Comparing the mechanical properties of the solid solution alloy and the as-cast alloy, it is found that UTS and EL increased by 7.8% and 85.7%, respectively, while TYS only decreased by 3.9%, and the comprehensive mechanical properties improved. Compared with room temperature, the mechanical properties of solid solution alloys at elevated temperatures decreased by only 9.9% and 1.78% for TYS and UTS, while EL increased by 58.9%. This suggests that solid solution alloy has good high-temperature stability. The serrated flow characteristics can be observed in the Alloy C curve, which may be caused by the Portevin-Le Chatelier (PLC) effect of Alloy C during stretching [30].

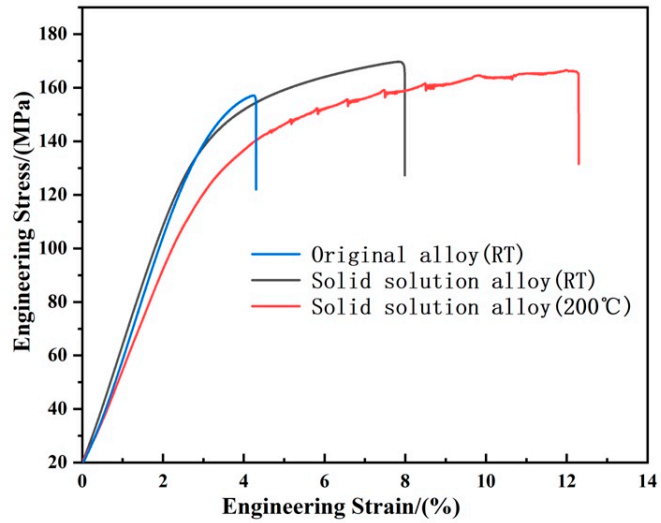


Figure 9. Engineering stress–strain curves of different alloys.

Figure 10 shows the tensile fracture morphologies of the Mg-1Al-12Y alloy under three tensile conditions. The fracture surface of Alloy A (Figure 10a) consists of larger cleavage planes and a tearing ridge, showing a typical brittle fracture mode. The fracture surface of Alloy B (Figure 10c) consists of smaller cleavage planes, small and shallow dimples and

a tearing ridge, showing a fracture morphological pattern of quasi-dissociative fracture. The number of cleavage planes of Alloy C (Figure 10e) is greatly reduced, the number and depth of dimples are also greatly improved, and the fracture mode is the same as that of Alloy B, but the toughness is improved. Figure 10b, d and f are high-magnification SEM images of Figure 10a,c, and e. In the high-magnification fracture SEM images, it is found that there are large-sized particles on the fracture surface. The point scan EDS image shown in Figure 10g indicates that these large-sized particles are Al_2Y phase particles. These Al_2Y phase particles still maintain their original morphology without deformation or cracking. These Al_2Y phases belonging to the hard phase have a dual effect on the mechanical properties of the material. On the one hand, they have the effect of hindering the movement of dislocations, resulting in the improvement of the material strength. On the other hand, due to the large difference between the elastic modulus of the LPSO phase and α-Mg matrix, the stress is concentrated at the intersection of the two, which inevitably becomes the fragmentation nucleation site [31].

Table 1. Mechanical properties of alloys under different tensile conditions.

Alloy	A	B	C
TYS MPa	133.45	128.2	115.39
UTS MPa	156.99	169.27	166.26
Elongation %	4.2	7.8	12.4

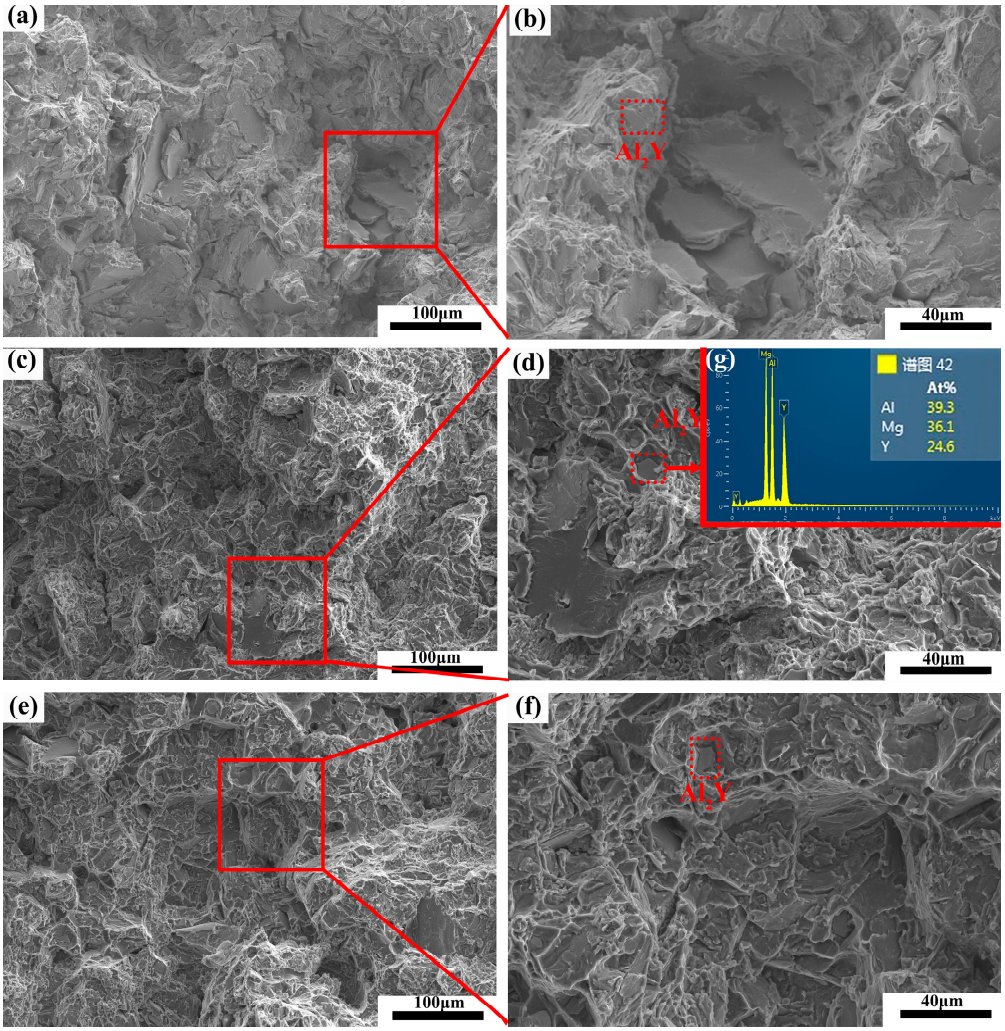


Figure 10. The SEM images of tensile fractures of Mg-1Al-12Y alloy under different tensile conditions: (**a**,**b**) alloy A, (**c**,**d**) alloy B, (**e**,**f**) alloy C, (**g**) EDS image.

4. Discussion

According to the observation, it can be found that the grain size of as-cast Mg-1Al-12Y alloy after solution treatment and the size and location of the Al_2Y phase have not obviously changed, and β-$Mg_{24}Y_5$ phase disappears, and the LPSO phase precipitates. These observations contributed to further analyzing the strengthening of room temperature mechanical properties of Mg-1Al-12Y solid solution alloy and its high-temperature stability. Therefore, further discuss as follows:

As shown in Figure 4, it can be found that the grain size of Mg-1Al-12Y alloy only slightly increases after solution treatment, which is not obvious. Figures 2b and 3d show that the β-$Mg_{24}Y_5$ phase in the alloy is dissolved, and the LPSO phase is precipitated after solution treatment. Meanwhile, it can be observed that the comprehensive mechanical properties of Alloy B have been greatly improved compared with Alloy A. The mechanical properties of solid solution alloy at high temperatures have only slightly decreased compared with room temperature, with good high-temperature stability, as shown in Figure 9. Hence, the improvement of mechanical properties and high-temperature stability of the alloy is not related to the change in grain size but is significantly related to the LPSO phase in the alloy.

The second-phase particles have a very complex effect on the mechanical properties, which are related to the morphology, sizes and distribution of the second phase. Generally, the dispersive distribution of the second phase favors an increase in strength. Since the LPSO phase is formed on the (0001) plane, the resulting strengthening can be calculated according to the Orowan relationship, as shown in Equation (1) below [32]:

$$\Delta\sigma_{Orowan} = \frac{MG_m b}{2\pi\lambda\sqrt{1-\nu}} \ln\frac{d_p}{r_0} \quad (1)$$

where M (= 4.5 for the pure Mg) is Taylor factor, G_m (= 16.6 GPa) is the shear modulus of Mg matrix, b (= 0.32 nm) is Burgers vector of base slip, λ is effective plane obstacle spacing, ν (= 0.35) is Poisson's ratio, d_p is the average diameter of LPSO phase and r_0 is the core radius of dislocation. For the convenience of expression, it is assumed that $r_0 = b$. λ can be expressed as.

$$\lambda = \left(\frac{0.953}{\sqrt{f}} - 1\right) d_p \quad (2)$$

where d_p is the average diameter of the LPSO phase and f is the volume fraction of the LPSO phase in the alloy. Alloy B precipitates the intragranular dispersed LPSO phase and the interdendritic LPSO phase after solution treatment. When the average length of the dendrite the LPSO phase fiber in the alloy is less than 30 μm, the LPSO fiber cannot provide the reinforcement effect [33]. The results show that the average length of the dendrite LPSO phase in the solid solution alloy is ~12.17 μm, so it cannot provide a significant short fiber strengthening effect. The parameters used for the Orowan relationship were measured. The average diameters of the lamellar LPSO phase and dendritic LPSO phase were ~0.85 μm and ~1.62 μm, respectively, and the area fractions are ~0.1961 and ~0.00686, respectively. According to Equations (1) and (2), it is calculated that the increment provided by the intragranular LPSO phase and interdendritic LPSO phase is 38.0020 MPa and 2.3649 MPa, respectively. The results show that the intragranular LPSO phase precipitated from the alloy after solution treatment has a good strengthening effect, while the interdendritic LPSO phase provides no obvious strengthening effect.

The IPF image of the three tensile samples is shown in Figure 11. It is found that the alloy grains after tension have no preferred orientation. Due to the formation of a large number of dispersed lamellar LPSO phases inside the grains of Alloy B, the TYS of Alloy B is theoretically higher than that of Alloy A. However, the TYS of Alloy B and Alloy C are lower than Alloy A in the experimental results, while the UTS and ductility have greatly improved. Since the α-Mg/LPSO phase interface hinders the movement of dislocations, stress concentration and uncoordinated strain occur in Alloy B and Alloy C, resulting in a

decrease in the TYS of Alloy B and Alloy C. The Schmid factor (SF) distributions of the basal slip for the three tensile samples are shown in Figure 12. Typically, basal <a> slip is more easily activated with higher mean SF values, resulting in lower yield strength and higher ductility, and vice versa [34]. In this paper, the average SF value of Alloy B is higher than that of Alloy A, so Alloy B has a comparatively lower yield strength and higher ductility. However, the average SF value of Alloy C is slightly lower than that of Alloy A and Alloy B. Namely, Alloy C should have higher yield strength and ductility, which is contrary to the experimental results. Therefore, in addition to the second phase and basal <a> slip, other factors affect the ductility of solid solution alloys at elevated temperatures.

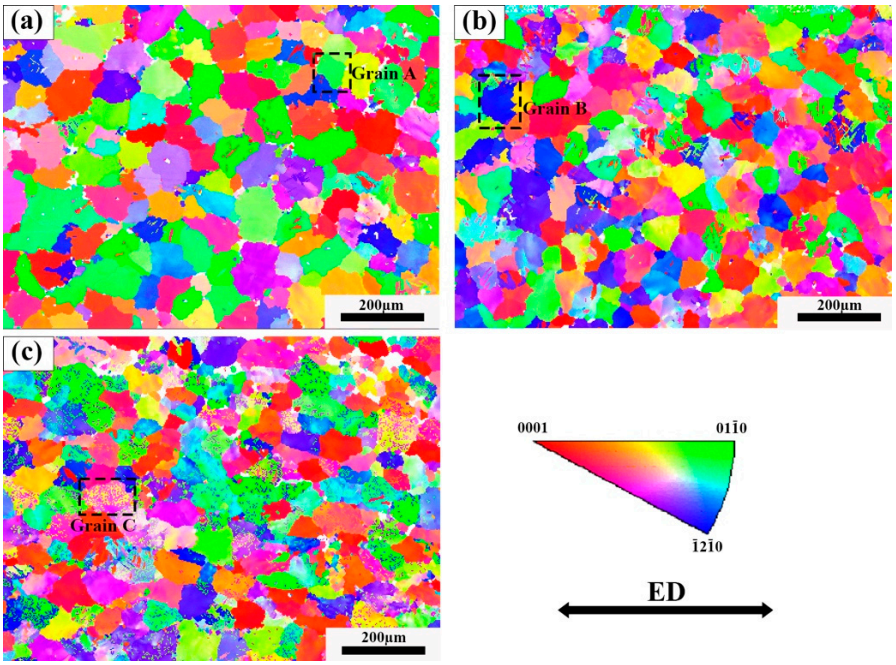


Figure 11. IPF diagram near the fracture after stretching, (**a**) Alloy A, (**b**) Alloy B, (**c**) Alloy C.

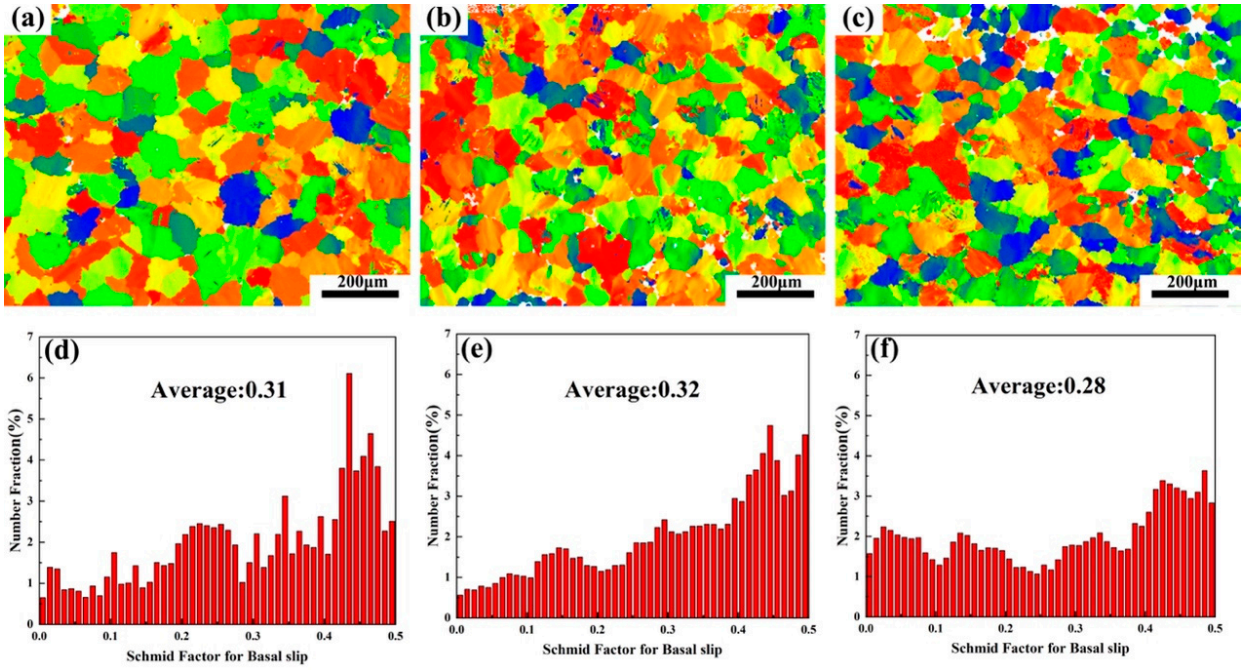


Figure 12. Basal slip Schmid factor (SF) distribution of three alloys: (**a**,**d**) Alloy A, (**b**,**e**) Alloy B, (**c**,**f**) Alloy C.

At room temperature, few slip systems can be started, which cannot coordinate the stress along the c-axis. The main deformation mechanism of Mg alloys during room temperature deformation is base slip and tension twins. It can be found that many twins appear in the microstructure of Alloy A and Alloy B, while almost no twins appear in Alloy C (Figure 11). Alloy C has no twins because twins' formation in grains with a high-density LPSO phase is inhibited [22]. Then, a crystal grain without twins and no second phase was selected from each sample, denoted as grains A, B and C, respectively. Figure 13 shows IPF and KAM images for grains A, B, and C. The stress in grain A is mainly concentrated at the grain boundaries (Figure 13a). However, in grain B, the grain boundary and the LPSO phase interface inside the grain appear to have stress concentration (Figure 13b), which is due to the hindering effect of the α-Mg/LPSO interface on dislocation slip [7,35], which is a good barrier. As shown in Figure 13c, stress concentration does not occur near the LPSO phase outside the grains, while stress concentration occurs near the LPSO phase distributed inside the grains, which is due to the kinking of part of the LPSO phase during stretching. Kinks of the LPSO phase will lead to the improvement of plastic deformation and is conducive to the improvement of ductility [36].

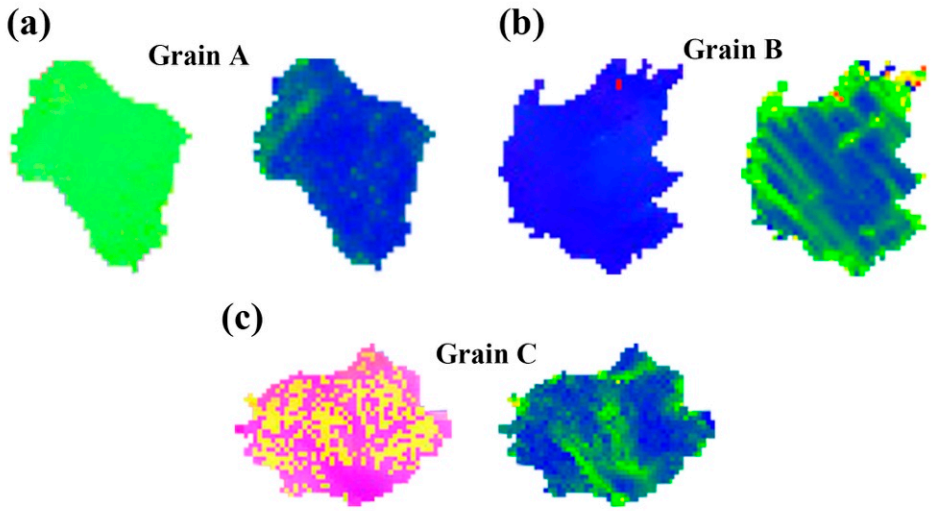


Figure 13. Select Grain A, B and C without twins and the second phase from Alloy A, B and C in Figure 11. IPF image and Kernel average misorientation (KAM) maps of grans: (**a**) Grain A, (**b**) Grain B, (**c**) Grain C.

Figure 14 shows the KAM and grain boundary images near the fracture of the three tensile samples. Figure 14a–c shows the KAM images. Alloy A exhibits the lowest KAM value (0.7), indicating the lowest local misorientation [37]. The KAM value of Alloy B is much higher than that of Alloy A, which is not conducive to improving ductility in theory. However, the experimental results are contrary to it. This is due to the α-Mg/LPSO interface being an effective barrier to hinder the movement of dislocations, and a lot of dislocations accumulate inside the grains, which slows down the failure process of Alloy B grain boundaries due to stress concentration and improves the UTS and ductility of Alloy B. As shown in Table 2, compared with Alloy B, Alloy C exhibits a lower KAM value (1.13) and higher LAGBs (61.7%), which is beneficial to the increase in ductility [38]. Figure 15 shows the SF profiles of the pyramidal <c + a> slip for three tensile samples. The average SF value of pyramidal slip in Alloy C is higher than that in Alloy B, indicating that more pyramidal <c + a> slip is activated in Alloy C, non-basal slip can promote more uniform deformation of grains and reduce stress concentration, which is also conducive to the increase in ductility [39–41].

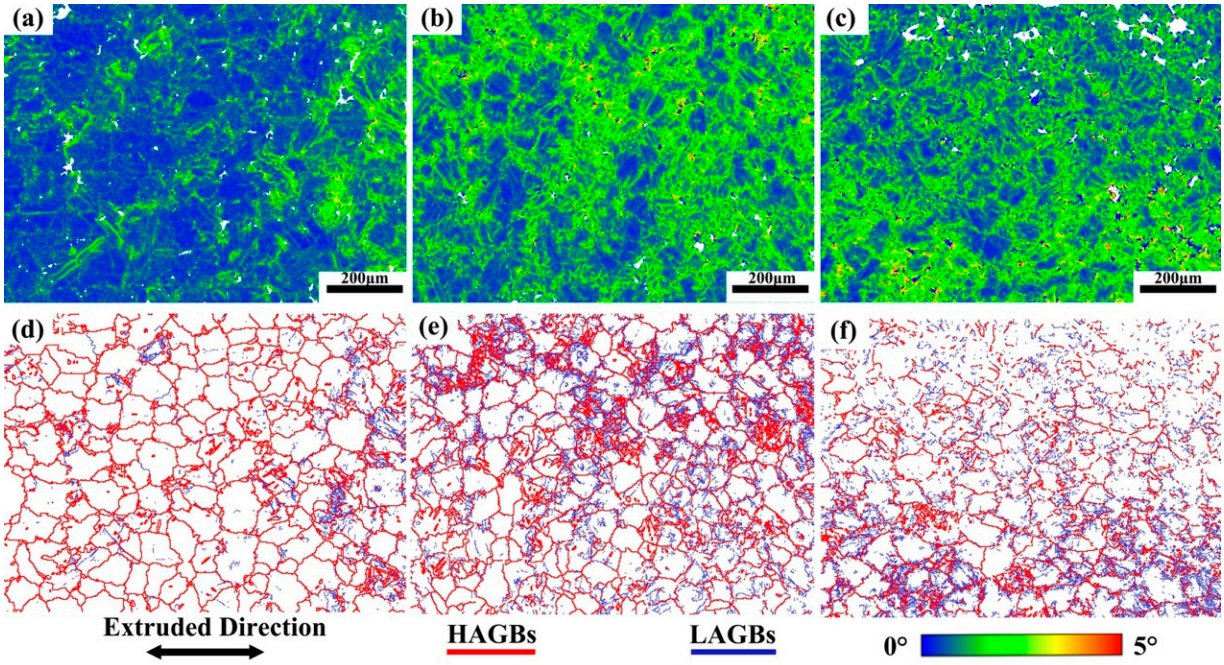


Figure 14. KAM diagram and grain boundary diagram near the alloy fracture, (**a**,**d**) Alloy A, (**b**,**e**) Alloy B, (**c**,**f**) Alloy C.

Table 2. EBSD data table of alloys with different tensile conditions.

Alloy	A	B	C
AKAM	0.7	1.14	1.13
HAGBs %	70	47.6	38.3
LAGBs %	30	52.4	61.7

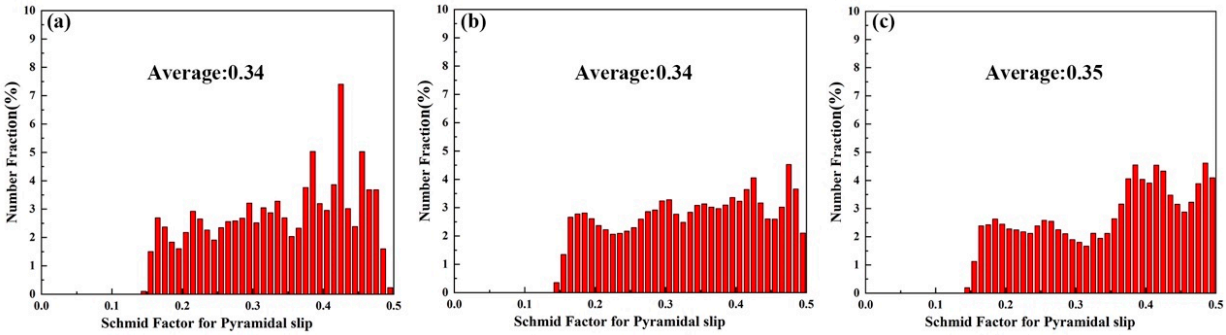


Figure 15. The pyramidal <c + a> slip SF distribution of three alloys, (**a**) Alloy A, (**b**) Alloy B, (**c**) Alloy C.

5. Conclusions

By studying the precipitation law and mechanical properties of the LPSO phase in Mg-1Al-12Y alloy, the following conclusions can be drawn:

There are three phases in the as-cast Mg-1Al-12Y alloy, which are the α-Mg matrix, Al_2Y phase and β-$Mg_{24}Y_5$ phase. After solution treatment, the grain size and Al_2Y phase in the alloy did not change significantly, the β-$Mg_{24}Y_5$ phase dissolved and the LPSO phase precipitated. The precipitation rule of the LPSO phase in as-cast Mg-1Al-12Y alloy is that at the same solution temperature, with the extension of solution time, the area fraction of the LPSO phase precipitated in the alloy increases correspondingly.

Compared with as-cast alloys, the room temperature mechanical properties of solid solution alloys increased by ~7.8% and ~85.7% in UTS and EL and decreased by ~3.9%

in TYS. The comprehensive mechanical properties were improved. Compared with room temperature, the mechanical properties of solid solution alloy at high temperature only decreased by ~9.9% and ~1.78% for TYS and UTS but increased by ~58.9% for EL, showing good high-temperature stability.

The improvement of the comprehensive mechanical properties of solid solution alloys at room temperature is due to the dispersion strengthening caused by the intragranular LPSO phase dispersed in the alloy. LPSO has a good blocking effect on dislocation slip and more basal <a> slip initiation.

The ductility of Mg-1Al-12Y alloy is improved at high temperatures while maintaining high strength due to the kink phenomenon, the reduction in dislocation density, and more non-basal slip activation.

Author Contributions: Conceptualization, J.W., W.L. and L.W.; Data curation, Q.R.; Formal analysis, Q.R.; Methodology, J.W. and D.M.; Software, Q.R.; Supervision, S.Y. and J.W.; Validation, S.Y.; Writing—original draft, Q.R.; Writing—review and editing, S.Y. All authors have read and agreed to the published version of the manuscript.

Funding: This research received no external funding.

Data Availability Statement: Not applicate.

Acknowledgments: Authors acknowledge the financial support of Qinghai Provincial Key Laboratory of New Light Alloys (No. 2022-ZJ-Y20) to carry out this research work.

Conflicts of Interest: The authors declare no conflict of interest.

References

1. Pollock, T.M. Weight Loss with Magnesium Alloys. *Science* **2010**, *328*, 986–987. [CrossRef] [PubMed]
2. Hwang, J.H.; Zargaran, A.; Park, G.; Lee, O.; Lee, B.-J.; Kim, N.J. Effect of 1Al addition on deformation behavior of Mg. *J. Magnes. Alloy.* **2021**, *9*, 489–498. [CrossRef]
3. Wang, Q.; Jiang, B.; Chen, D.; Jin, Z.; Zhao, L.; Yang, Q.; Huang, G.; Pan, F. Strategies for enhancing the room-temperature stretch formability of magnesium alloy sheets: A review. *J. Mater. Sci.* **2021**, *56*, 12965–12998. [CrossRef]
4. Jung, Y.-G.; Yang, W.; Kim, Y.J.; Kim, S.; Yoon, Y.-O.; Lim, H.; Kim, D.H. Effect of Ca addition on the microstructure and mechanical properties of heat-treated Mg-6.0Zn-1.2Y-0.7Zr alloy. *J. Magnes. Alloy.* **2021**, *9*, 1619–1631. [CrossRef]
5. Chaudry, U.M.; Tekumalla, S.; Gupta, M.; Jun, T.-S.; Hamad, K. Designing highly ductile magnesium alloys: Current status and future challenges. *Crit. Rev. Solid State Mater. Sci.* **2021**, *47*, 194–281. [CrossRef]
6. Yokobayashi, H.; Kishida, K.; Inui, H.; Yamasaki, M.; Kawamura, Y. Enrichment of Gd and Al atoms in the quadruple close packed planes and their in-plane long-range ordering in the long period stacking-ordered phase in the Mg–Al–Gd system. *Acta Mater.* **2011**, *59*, 7287–7299. [CrossRef]
7. Mayama, T.; Agnew, S.R.; Hagihara, K.; Kamura, K.; Shiraishi, K.; Yamasaki, M.; Kawamura, Y. α-Mg/LPSO (Long-Period Stacking Ordered) phase interfaces as obstacles against dislocation slip in as-cast Mg-Zn-Y alloys. *Int. J. Plast.* **2022**, *154*, 103294. [CrossRef]
8. Yin, W.; Briffod, F.; Shiraiwa, T.; Enoki, M. Mechanical properties and failure mechanisms of Mg-Zn-Y alloys with different extrusion ratio and LPSO volume fraction. *J. Magnes. Alloy.* **2022**, *10*, 2158–2172. [CrossRef]
9. Gu, X.-F.; Furuhara, T.; Chen, L.; Yang, P. Domain structures and the transitional state of ordering in long-period stacking ordered (LPSO) structures in Mg–Al–Gd alloy. *Scr. Mater.* **2020**, *187*, 19–23. [CrossRef]
10. Kim, H.; Ross, A.J.; Shang, S.-L.; Wang, Y.; Kecskes, L.J.; Liu, Z.-K. First-principles calculations and thermodynamic modelling of long periodic stacking ordered (LPSO) phases in Mg-Al-Gd. *Materialia* **2018**, *4*, 192–202. [CrossRef]
11. Wang, Y.; Zhang, Y.; Wang, P.; Zhang, D.; Yu, B.; Xu, Z.; Jiang, H. Effect of LPSO phases and aged-precipitations on corrosion behavior of as-forged Mg–6Gd–2Y–1Zn–0.3Zr alloy. *J. Mater. Res. Technol.* **2020**, *9*, 7087–7099. [CrossRef]
12. Jeong, H.T.; Kim, W.J. The hot compressive deformation behavior of cast Mg-Gd-Y-Zn-Zr alloys with and without LPSO phase in their initial microstructures. *J. Magnes. Alloy.* **2022**, *10*, 2901–2917. [CrossRef]
13. Hao, Y.; Chen, X.; Zhao, Z.; Chen, Z.; Chen, B. The interface between long-period stacking-ordered (LPSO) structure and β′ phase in Mg-Gd-Al alloys. *J. Alloy. Compd.* **2022**, *923*, 166267. [CrossRef]
14. Nishimoto, S.; Koguchi, Y.; Yamasaki, M.; Kawamura, Y. Effect of hierarchical multimodal microstructure evolution on tensile properties and fracture toughness of rapidly solidified Mg–Zn–Y–Al alloys with LPSO phase. *Mater. Sci. Eng. A* **2022**, *832*, 142348. [CrossRef]
15. Yang, Q.; Guan, K.; Li, B.; Meng, F.; Lv, S.; Yu, Z.; Zhang, X.; Zhang, J.; Meng, J. Coexistence of 14H and 18R-type long-period stacking ordered (LPSO) phases following a novel orientation relationship in a cast Mg−Al−RE−Zn alloy. *J. Alloy. Compd.* **2018**, *766*, 902–907. [CrossRef]

16. Shi, R. Nonisothermal dissolution kinetics on Mg17Al12 intermetallic in Mg-Al alloys. *J. Magnes. Alloy.* **2021**, *10*, 2421–2432. [CrossRef]
17. Korgiopoulos, K.; Pekguleryuz, M. The significant effect of trace yttrium level on the mechanical properties of cast Mg–6Al alloy through a refinement mechanism. *Mater. Sci. Eng. A* **2020**, *775*, 138966. [CrossRef]
18. Wang, J.H. Study on Static and Dynamic Mechanical Behavior of Mg-Al-Y Alloys. Ph.D. Thesis, Shenyang University of Technology, Shenyang, China, 2021. [CrossRef]
19. Li, Y.; Yang, C.; Zeng, X.; Jin, P.; Qiu, D.; Ding, W. Microstructure evolution and mechanical properties of magnesium alloys containing long period stacking ordered phase. *Mater. Charact.* **2018**, *141*, 286–295. [CrossRef]
20. Hagihara, K.; Okamoto, T.; Izuno, H.; Yamasaki, M.; Matsushita, M.; Nakano, T.; Kawamura, Y. Plastic deformation behavior of 10H-type synchronized LPSO phase in a Mg–Zn–Y system. *Acta Mater.* **2016**, *109*, 90–102. [CrossRef]
21. Jiang, M.; Zhang, S.; Bi, Y.; Li, H.; Ren, Y.; Qin, G. Phase equilibria of the long-period stacking ordered phase in the Mg–Ni–Y system. *Intermetallics* **2015**, *57*, 127–132. [CrossRef]
22. Nie, J.F.; Zhu, Y.M.; Morton, A.J. On the Structure, Transformation and Deformation of Long-Period Stacking Ordered Phases in Mg-Y-Zn Alloys. *Met. Mater. Trans. A* **2014**, *45*, 3338–3348. [CrossRef]
23. Peng, Z.; Shao, X.; Liang, Z.; Wang, D.; Wang, L.; Ma, X. Synergetic deformation mechanisms in an Mg-Zn-Y-Zr alloy with intragranular LPSO structures. *J. Magnes. Alloy.* **2022**. [CrossRef]
24. Matsuda, M.; Ii, S.; Kawamura, Y.; Ikuhara, Y.; Nishida, M. Variation of long-period stacking order structures in rapidly solidified $Mg_{97}Zn_1Y_2$ alloy. *Mater. Sci. Eng. A* **2005**, *393*, 269–274. [CrossRef]
25. Chen, Y.; Li, Q.; Li, Y.; Zheng, W.; Wang, J.; Zeng, X. Phase equilibria of long-period stacking ordered phase in the ternary Mg-Y-Al alloys. *J. Mater. Sci. Technol.* **2022**, *126*, 80–92. [CrossRef]
26. Yuan, S.; Wang, J.; Li, X.; Ma, H.; Zhang, L.; Jin, P. Enhanced mechanical properties of Mg-1Al-12Y alloy containing long period stacking ordered phase. *J. Magnes. Alloy.* **2022**. [CrossRef]
27. Zhu, Q.; Shang, X.; Zhang, H.; Qi, X.; Li, Y.; Zeng, X. Influence of Al_2Y particles on mechanical properties of Mg-11Y-1Al alloy with different grain sizes. *Mater. Sci. Eng. A* **2022**, *831*, 142166. [CrossRef]
28. Su, C.; Wang, J.; Hu, H.; Wen, Y.; Liu, S.; Ma, K. Enhanced strength and corrosion resistant of Mg-Gd-Y-Al alloys by LPSO phases with different Al content. *J. Alloy. Compd.* **2021**, *885*, 160557. [CrossRef]
29. Kim, J.; Kawamura, Y. Influence of Rare Earth Elements on Microstructure and Mechanical Properties of $Mg_{97}Zn_1Y_1RE_1$ Alloys. *Mater. Sci. Eng. A* **2013**, *573*, 62–66. [CrossRef]
30. Hu, Z.; Qi, Y.; Nie, X.; Zhang, H.; Zhu, H. The Portevin-Le Chatelier (PLC) effect in an Al-Cu aluminum alloy fabricated by selective laser melting. *Mater. Charact.* **2021**, *178*, 111198. [CrossRef]
31. Sun, H.-F.; Li, C.-J.; Fang, W.-B. Evolution of microstructure and mechanical properties of Mg–3.0Zn–0.2Ca–0.5Y alloy by extrusion at various temperatures. *J. Mater. Process. Technol.* **2016**, *229*, 633–640. [CrossRef]
32. Li, C.; Liu, H.; Xin, Y.; Guan, B.; Huang, G.; Wu, P.; Liu, Q. Achieving ultra-high strength using densely ultra-fine LPSO phase. *J. Mater. Sci. Technol.* **2022**, *129*, 135–138. [CrossRef]
33. Hagihara, K.; Kinoshita, A.; Sugino, Y.; Yamasaki, M.; Kawamura, Y.; Yasuda, H.; Umakoshi, Y. Effect of long-period stacking ordered phase on mechanical properties of Mg97Zn1Y2 extruded alloy. *Acta Mater.* **2010**, *58*, 6282–6293. [CrossRef]
34. del Valle, J.; Carreño, F.; Ruano, O. Influence of texture and grain size on work hardening and ductility in magnesium-based alloys processed by ECAP and rolling. *Acta Mater.* **2006**, *54*, 4247–4259. [CrossRef]
35. Li, C.; Malik, A.; Nazeer, F.; Chaudry, U.M.; Long, J.; Wang, Y. A strong, ductile and in-plane tensile isotropic Mg-0.5Zn-0.5Y-0.15Si alloy. *J. Mater. Res. Technol.* **2022**, *20*, 3344–3354. [CrossRef]
36. Gong, W.; Aizawa, K.; Harjo, S.; Zheng, R.; Kawasaki, T.; Abe, J.; Kamiyama, T.; Tsuji, N. Deformation behavior of as-cast and as-extruded $Mg_{97}Zn_1Y_2$ alloys during compression, as tracked by in situ neutron diffraction. *Int. J. Plast.* **2018**, *111*, 288–306. [CrossRef]
37. Yamasaki, S.; Tokuzumi, T.; Li, W.; Mitsuhara, M.; Hagihara, K.; Fujii, T.; Nakashima, H. Kink Formation Process in Long-Period Stacking Ordered Mg-Zn-Y Alloy. *Acta Mater.* **2020**, *195*, 25–34. [CrossRef]
38. Pan, H.; Kang, R.; Li, J.; Xie, H.; Zeng, Z.; Huang, Q.; Yang, C.; Ren, Y.; Qin, G. Mechanistic investigation of a low-alloy Mg–Ca-based extrusion alloy with high strength–ductility synergy. *Acta Mater.* **2020**, *186*, 278–290. [CrossRef]
39. Zhao, D.; Chen, X.; Li, J.; Tan, J.; Pan, F. Microstructure, texture and mechanical properties of the rolled high modulus Mg-Y-Zn-Al-Li alloy. *Mater. Sci. Eng. A* **2022**, *831*, 142242. [CrossRef]
40. Yuan, S.; Wang, J.; Zhang, L.; Jin, P. An investigation of the deformation and cracking mechanism of Mg–1Al–12Y alloys based on in-situ SEM/EBSD slip trace analysis. *Mater. Sci. Eng. A* **2022**, *856*, 144016. [CrossRef]
41. Chaudry, U.M.; Hamad, K.; Kim, J.-G. On the ductility of magnesium based materials: A mini review. *J. Alloy. Compd.* **2019**, *792*, 652–664. [CrossRef]

Disclaimer/Publisher's Note: The statements, opinions and data contained in all publications are solely those of the individual author(s) and contributor(s) and not of MDPI and/or the editor(s). MDPI and/or the editor(s) disclaim responsibility for any injury to people or property resulting from any ideas, methods, instructions or products referred to in the content.